Chemistry Faculty Research & Creative Works   Chemistry

01 Sep 2015

Generalized Synthesis of EAs [E = Fe, Co, Mn, Cr] Nanostructures and Investigating their Morphology Evolution

Prachi Desai

Nikitaa Ashokan

Manashi Nath
Missouri University of Science and Technology, nathm@mst.edu

Recommended Citation

Research Article

Generalized Synthesis of *E*As [*E* = Fe, Co, Mn, Cr] Nanostructures and Investigating Their Morphology Evolution

P. Desai,[1] **Nikitaa Ashokan,**[2] **and M. Nath**[1]

[1]*Department of Chemistry, Missouri University of Science & Technology, Rolla, MO 65409, USA*
[2]*Department of Chemical and Biochemical Engineering, Missouri University of Science & Technology, Rolla, MO 65409, USA*

Correspondence should be addressed to M. Nath; nathm@mst.edu

Academic Editor: Chuanbao Cao

This paper illustrates a novel route for the synthesis of nanostructured transition metal arsenides including those of FeAs, CoAs, MnAs, and CrAs through a generalized protocol. The key feature of the method is the use of one-step *hot-injection* and the clever use of a combination of precursors which are low-melting and highly reactive such as metal carbonyls and triphenylarsine in a solventless setup. This method also facilitates the formation of one-dimensional nanostructures as we move across the periodic table from CrAs to CoAs. The chemical basis of this reaction is simple redox chemistry between the transition metals, wherein the transition metal is oxidized from elemental state (E^0) to E^{3+} *in lieu* of reduction of As^{3+} to As^{3-}. While the thermodynamic analysis reveals that all these conversions are spontaneous, it is the kinetics of the process that influences morphology of the product nanostructures, which varies from extremely small nanoparticles to nanorods. Transition metal pnictides show interesting magnetic properties and these nanostructures can serve as model systems for the exploration of their intricate magnetism as well as their applications and can also function as starting materials for the arsenide based nanosuperconductors.

1. Introduction

Metal pnictides are an important class of compounds exhibiting interesting electronic, semiconducting, optical, and magnetic properties [1]. For the last decade a major emphasis for pnictides was laid on main group metal phosphides and arsenides like InP, GaAs, and InAs. These have taken a center stage as a potential replacement to Si in applications related to electronics, optoelectronics, and photovoltaics [2]. More recently, the binary transition metal pnictides owing to their structures and magnetic properties have gained importance as semiconductors [3, 4], anode materials for Li-ion batteries [5], and novel magnetic materials [6]. Amongst the arsenides, CrAs is a half-metallic ferromagnet with a band gap of 1.8 eV [7] while MnAs also shows ferromagnetic interactions [8]. Such ferromagnetic semiconductors are important in the field of spintronics. MnAs is also known to have a large electromotive force that can be used to convert magnetic energy to electrical energy when used as components of circuits [8]. FeAs, on the other hand, is a helimagnet [9] with helical arrangement of spins associated with Fe atoms

which has an overall antiferromagnetic ordering below 77 K. It was found that the ferromagnetic order is more stable than the antiferromagnetic state for VAs, CrAs, and MnAs, the greatest energy gain being predicted for CrAs [10]. Some of these transition metal pnictide also belong to the structure type of filled skutterudite (typically Co_3As) which shows promise as thermoelectric materials [11]. The mixed arsenides like $MnAs_{(1-x)}P_x$ [12] are also useful as thermoelectrics. Apart from the binaries, other mixed metal phosphides containing two or more transition metals have been used to improve the fire safety properties of polypropylene [13]. Other applications also include their usage as important catalysts for hydrodenitrogenation (HDN), hydrodesulfurization (HDS), and hydroprocessing of specialty chemicals [14–17] especially with transition metal phosphides. The role of enhanced surface area with nanostructuring and exposed crystal faces has increased their effectiveness in catalysis whereby metal phosphides nanoparticles (Ni_2P) have been used as electrocatalysts for hydrogen evolution reactions [18]. Apart from the interesting magnetic and electronic properties associated
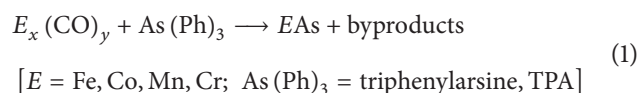
with them, the arsenides have also gained attention following the recent discovery of Fe-based superconductors containing both FeP/FeAs tetrahedral layers and intercalating layers of oxides/alkali metals/alkaline earths [19]. It was observed that magnetic ordering plays an important role in these superconducting transition metal pnictides. Superconductivity was typically observed at the vicinity of the magnetically ordered phase and tuning the magnetic properties through doping or introducing lattice deformities was found to have a profound effect on the superconductivity. Transition metal pnictide nanoparticles are thereby interesting owing to their interesting electronic and magnetic properties which can offer valuable insight into the structure-property relationship.

While transition metal phosphides have been researched by various groups, in spite of the plethora of useful applications, there has been a lack of a rationalized synthesis protocol for the transition metal arsenides [20–22]. This dearth of synthetic strategy has been mainly attributed to the toxic nature of arsenic salts which limits the range of useable precursors and also the reaction conditions. Nanostructuring of transition metal arsenides has been explored before by Lu et al. [23] who have made FeAs nanoparticles sonochemically from transition metal chlorides and arsenic while Zhang and coworkers [24] made FeAs nanocrystals from reductive recombination of $FeCl_3$ and $AsCl_3$ at 150–180°C. Another interesting approach involved reduction of pnictate precursors to produce the pnictides. However, this approach only produced bulk forms of the pnictides [25]. All of these methods involved toxic precursors or solvents. Since sustainability and green synthesis of nanomaterials have been one of the greatest concerns amongst researchers these days, there is a need for developing synthesis protocols for these functional nanostructures using less toxic reagents. To this cause, regulated/minimal usage of hydrocarbon based solvents in synthetic methods has been pushed as a way to synthesize "green" nanoparticles. We have devised one such approach which does not involve any additional solvent at the time of synthesis. Rather it takes advantage of the reducing ability of the capping agent, which itself melts and forms a molten flux-like medium and maintains a basic environment under the synthesis conditions. This approach is a proof that solvents in many nanoparticle syntheses may be redundant and can be totally eliminated if clever reaction precursors and conditions are applied. Hence, with this method reported in this paper we can positively address the sustainability cause for synthesis methods which involve solvent based nanoparticle synthesis approaches. This was the key motivation behind developing this process. It should be noted, however, that minimal solvents are required during the purification step due to the magnetic nature of these nanostructured transition metal arsenides. The generalized facile synthesis route to the transition metal arsenides is based on our previous report on the synthesis of superparamagnetic FeAs and soft ferromagnetic CoAs nanoparticles [26, 27]. Typically the synthesis process involves hot-injection of the metal precursor into a refluxing mixture of the arsenic precursor in presence of a surfactant, followed by prolonged refluxing. The nanostructures obtained by this method were mostly pure and we could also see a trend in the morphology evolution,

typically increasing anisotropy (i.e., from nanoparticles to nanorods) as the transition metal was varied from left to right of the periodic table.

2. Materials and Methods

2.1. Synthesis. The synthesis of EAs [E = Cr, Mn, Fe, Co] nanoparticles was carried out in a N_2 filled glove box containing less than 1 ppm of O_2. 1 mM of triphenylarsine (TPA) and 5 mM of hexadecylamine (HDA) were weighed and added to a three-neck round bottom flask equipped with a magnetic stir bar and air condenser. The mixture was slowly heated to 325°C during which the reactants slowly melted and the colorless mixture refluxed in its own vapors. 1 mM of the transition metal carbonyl salt [$Fe(CO)_5$/$Co_2(CO)_8$/$Mn_2(CO)_{10}$/$Cr(CO)_6$] maintained at room temperature was then injected using a syringe pump or as solid into the hot HDA + TPA mixture. Upon addition of the carbonyl precursor the solution immediately turned blackish with rapid evolution of gases. After 5 min the gases subsided and the black solution was left to reflux for variable length of time. After the desired refluxing time, heating was stopped and reaction was cooled down to room temperature. The chemical reaction can be written as

$$E_x(CO)_y + As(Ph)_3 \longrightarrow EAs + byproducts$$
$$[E = Fe, Co, Mn, Cr; \; As(Ph)_3 = triphenylarsine, TPA] \tag{1}$$

2.2. Purification. The as-synthesized solid product, by virtue of its attraction to a magnet, was purified through simple magnetic filtration. The isolated product was washed at least 3-4 times with ethanol and hexane using ultrasonication to remove excess HDA and any unreacted precursors. The powder collected from the bottom of the centrifuge tube was dried in air. The yield of the product was in excess of 90% compared to the amount of the metal carbonyl (i.e., $Fe(CO)_5$/$Co_2(CO)_8$/$Mn_2(CO)_{10}$) taken as the precursor. It should be noted here that of all the arsenides prepared by this method only the CrAs nanoparticles did not yield a solid precipitate. The product containing Cr-arsenide formed a black suspension which remained as a stable dispersion. The solid products were characterized further through powder X-ray diffraction (PXRD), scanning and transmission electron microscopy (SEM and TEM, resp.), X-ray photoelectron spectroscopy (XPS), and EDS.

2.3. Characterization

2.3.1. PXRD. The as-synthesized powder was finely ground and used for PXRD, which was carried out on a Philips Xpert diffractometer scanning in the 2θ range of 5 to 90°.

2.3.2. SEM and TEM. A Tecnai F20 microscope operating at 200 kV was used for TEM imaging while a dual beam Helios FIB microscope was used for SEM and STEM studies. Samples for TEM and STEM were made by dispersing as-synthesized arsenide nanoparticles in ethanol by ultrasonication for 30 min and adding drops from the diluted dispersion
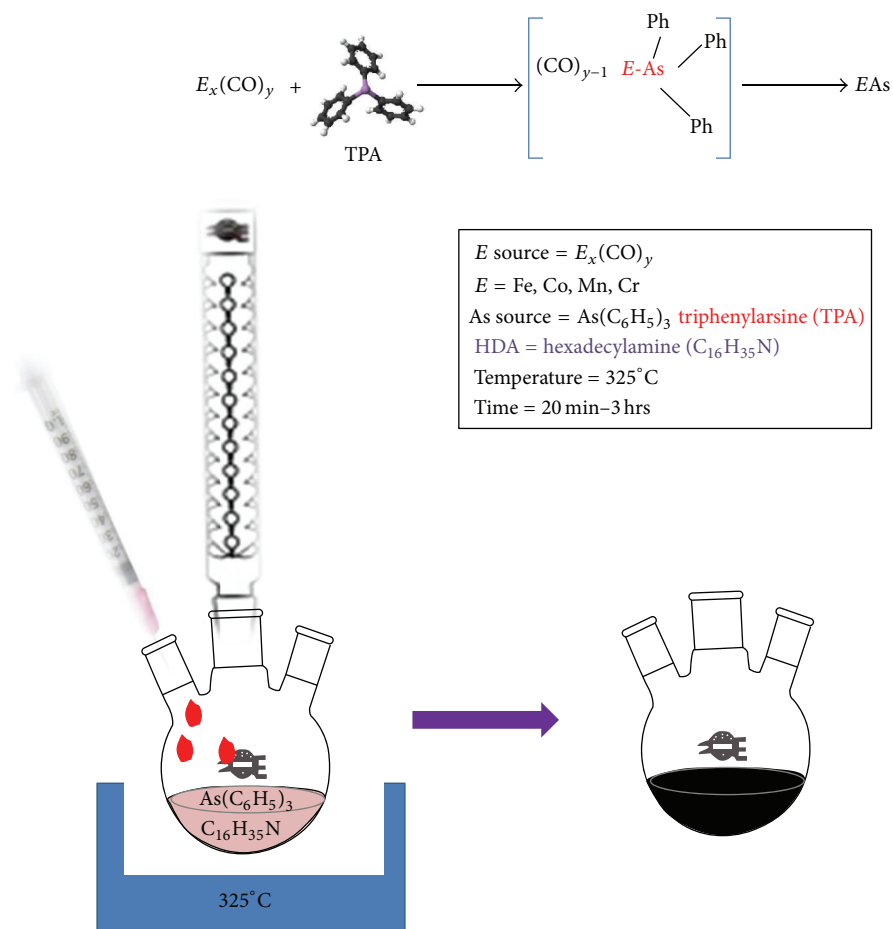
FIGURE 1: A schematic describing the synthesis protocol for the EAs nanostructures through hot-injection technique.

on a carbon coated 200-mesh Cu TEM grid followed by drying in air. For some arsenide nanostructures, the selected area electron diffraction (SAED) patterns were also collected in the TEM mode.

2.3.3. Magnetic Characterization.
Temperature-dependent magnetic moment at constant field and field-dependent isothermal magnetization measurements were performed with SQUID (superconducting quantum interference device) magnetometer. The powdered sample of a known mass (13.1 mg FeAs; 16.8 mg CoAs) was loaded in a gel cap, which was inserted into the magnetometer with the help of standard sample loader. Background signal was collected from the diamagnetic gel cap separately and subtracted from the sample signal. The isothermal magnetization at various temperatures (5 K, 100 K, and 300 K) was collected by varying applied magnetic field from −20,000 Oe to 20,000 Oe and recording the change in sample magnetization.

2.3.4. XPS.
XPS analysis was performed with Kratos Axis 165, with a hemispherical 8-channel analyzer. Photoemission was stimulated with a monochromatic Al source for FeAs@C and CoAs nanoparticles. The XPS spectra of Fe2p, Co2p, and As3d were collected at pass energy of 80 peV. Sputtering was performed for 2 min using argon gas.
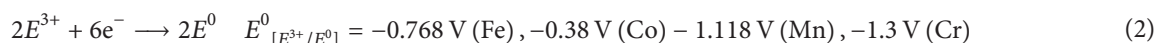
3. Results and Discussion

The synthesis was carried out by a facile *hot-injection* redox reaction under inert conditions. Figure 1 shows the general scheme of the reaction protocol. The central idea here was inducing rapid nucleation in homogeneous medium through *hot-injection* of the transition metal carbonyl in the presence of an arsine precursor. The arsine precursor chosen (TPA) was a low-melting, less volatile, precursor with less reducing power such that it offered control over the chemical reaction. It is known that very commonly used surfactant, hexadecylamine (HDA) containing a 16-C-atom chain, melts at 45°C and TPA melted at around 60°C. The mixture of TPA and HDA was heated to high temperatures. Under these conditions the melt behaved as a solvent by itself. The concept is similar to the flux-mediated synthesis conditions for solid-state reactions where a low-melting reagent is used as a flux to facilitate reactant diffusion and intimate mixing. After conducting several blank experiments without the metal precursors an appropriate temperature range was selected for injecting the metal carbonyls. This

temperature was 325°C and was based on the fact that at this temperature the HDA + TPA mixture remained colorless and had just started to reflux vigorously. Various stoichiometric combinations ranging from 1:1 to 1:10 TPA:HDA were tried. The appropriate combination to yield nanostructures was chosen as 1:5. Excess HDA caused excessive froth build-up whereas 1:1 relative ratio of TPA:HDA did not leave enough liquid phases for the metal carbonyls to react. When the TPA + HDA mixture was at the appropriate refluxing temperature, metal carbonyl was injected into the hot reaction mixture. It was observed that the transition metal oxidation state in the precursor was also important in the sense that it must be in the elemental or 0 oxidation state to guide the appropriate redox chemistry (Table 1). When metal precursors with metal in the positive oxidation states were used, the arsenide formation was hindered. This was verified by many reactions involving precursors other than the carbonyls like acetylacetonates and halides. When iron acetylacetonate was used as a metal source it resulted in impure products with Fe_2As and $FeAs_2$ as impurities. Metal halides like $FeCl_3$, $CoCl_2$, and $MnCl_2$ on the other hand were very sluggish in reacting and the reactions never proceeded to completion. Mechanistically it can be expected that, during initial stage of the reaction, ligand exchange takes place as soon as $E_x(CO)_y$ is added to the mixture of TPA and HDA as seen in Figure 1, whereby the CO ligand is displaced by the $As(C_6H_5)_3$ to form an intermediate complex $[(C_6H_5)_3As\text{-}E_x(CO)_{y-1}]$ with generation of free CO. This kind of ligand exchange with phosphines and arsines is very well known in organometallic chemistry and is very favorable since they act as electron donating Lewis bases [28]. Another factor that influences these ligand exchange reactions is the ability of the ligand (triphenylarsine) to stabilize the lower oxidation state of the metal. While the pnictides can stabilize the lower valence state of the transition metal, the amine-based ligands, especially monodentate amines like HDA, are insufficient to stabilize the lower valence state. Additionally, the more

preferable binding of TPA with the metal center can also be explained through HSAB principle. According to the HSAB principle the binding ability of TPA is superior to HDA since As in the Ph_3As behaves as a soft base and N in RNH_2 is a hard base. The transition metal centers due to their lower oxidation state are soft acids. The soft-soft interaction will be favored when comparing relative binding abilities of TPA and HDA. As a result, even if the monodentate HDA links to the transition metal center by replacing one of the CO groups, it would be spontaneously replaced by TPA to give an energetically more favorable coordination complex as shown in Figure 1. This intermediate formed in principle can behave as a single source precursor for both E and As. This kind of intermediate in fact has been reported for Co- and Fe-based carbonyls and their structures have been solved using X-ray crystallography and spectroscopic methods [29, 30]. The intermediate brings As and E closer than what would be expected in a traditional solid-state method of EAs synthesis. Proximity of As and E in this intermediate renders the possibility of an internal redox between As and E. The driving force is the difference in the reduction potentials of E^{3+}/E^0 and As^{3+}/As^{3-} couples as shown in (2) and (3), respectively. The presence of amine (HDA) in the mixture makes the reaction medium slightly basic, thereby decreasing the reducing ability of the arsine compound. Since As^{3+}/As^{3-} has a more positive reduction potential, it acts as a stronger oxidizing agent, thereby oxidizing E^0 to E^{3+}, while being itself reduced to As^{3-}.

Temperature also plays a definitive role in this ligand exchange and internal redox reactions, since it was observed that, at low temperature, the product contained a mixture of FeAs and $FeAs_2$ (which contains Fe in the +2 oxidation state). The lower valent arsenides were also obtained as impurities (e.g., $CoAs_2$ for the CoAs system) under low reaction temperature.

The reactions can be summarized as follows:

$$2E^{3+} + 6e^- \longrightarrow 2E^0 \quad E^0_{[E^{3+}/E^0]} = -0.768\,\text{V (Fe)}, -0.38\,\text{V (Co)} - 1.118\,\text{V (Mn)}, -1.3\,\text{V (Cr)} \tag{2}$$

$$As^{3+} + 6e^- \longrightarrow As^{3-} \quad E^0_{[As(3+)/As(3-)]} = +0.345\,\text{V}, \tag{3}$$

where E = Fe, Co, Mn, and Cr, respectively.

Combining the redox potentials for the half-cell reactions (2) and (3) and calculating the net cell potential, E_{net} ($E_{net} = E_{ox} + E_{red}$), it was observed that E_{net} was positive for all of these reactions, indicating that all of these conversions were spontaneous and energetically favorable. Accordingly ΔG was negative for all of these reactions. However, thermodynamics does not give a clear idea about the kinetics of the reaction. Hence, although all of the conversions in this series are spontaneous, the rate of the formation of the arsenides may vary drastically among the transition metals leading to different rates of reaction.

The composition and morphology of these arsenide products were studied through PXRD, XPS, STEM, and TEM studies, respectively. Crystal structures of binary transition metal arsenides contain 3D networks of EAs_6 [E = transition metal] octahedra or trigonal prisms. They crystallize in 5 structure types of which FeAs, CoAs, and CrAs belong to the orthorhombic MnP structure type [31–33], while MnAs crystallizes with NiAs structure type [34].

Morphology of the synthesized nanostructures was studied in detail with SEM and TEM including SAED. TEM image in Figure 2(a) shows the high degree of monodispersity of the as-synthesized FeAs nanoparticles. The FeAs

TABLE 1: Comparison of the redox potentials and the associated ΔG values for the transition metals.

EAs	$E_{net} = E_{ox} + E_{red}$	$\Delta G = -[nFE_{net}]$
FeAs	1.113	$-6.678F$
CoAs	0.695	$-4.17F$
MnAs	1.463	$-8.778F$
CrAs	1.645	$-9.87F$

nanoparticles were found to be highly crystalline and as-synthesized nanoparticles crystallized in the MnP structure type [JCPDS file card number 01-076-0458] as revealed by their PXRD pattern shown in Figure 2(b). The diameter of these nanoparticles was calculated from Scherrer equation to be 13 nm. Figure 2(c) is the HRTEM of a single FeAs nanoparticle, which shows lattice fringes corresponding to the (110) lattice planes. The average size distribution was studied through histogram analysis as shown in Figure S1 in Supplementary Information in Supplementary Material available online at http://dx.doi.org/10.1155/2015/362152, which also corroborated the PXRD size determination. The selected area electron diffraction (SAED) pattern obtained from these nanoparticles also confirmed high degree of crystallinity (inset in Figure 2(c)). As was apparent from the TEM images, the particles were of core-shell morphology. Line scans through EDS confirmed that the shell was made up of mainly carbon while the core contained Fe and As. No other phase of FeAs or any other impurity was detected [26]. The size of the nanoparticles was dependent on the refluxing time. When the temperature of $Fe(CO)_5$ addition was reduced to 250°C a mixture of $FeAs_2$ and FeAs was obtained. Detailed characterization and property studies of the superparamagnetic FeAs nanoparticles have been reported by the authors previously [26].

The PXRD pattern suggests that pure-phase CoAs nanostructures (JCPDS-01-077-1351) were formed by this method as shown in Figure 3(a). Figures 3(b) and 3(c) show STEM images of CoAs nanostructures during different stages of growth. The propensity to form nanowires was seen to be much higher with CoAs. It was noted that in the case of CoAs this *hot-injection* method yielded one-dimensional nanostructures within the first 10 min of introducing $Co_2(CO)_8$ into the reaction mixture (Figure 3(a)). As the reaction progressed further (for approximately 40 min), longer CoAs nanorods were obtained uniformly in the product. Figure 2(c) shows the HRTEM image of a nanorod exhibiting lattice fringes of 2.57 Å (corresponding to (111) planes) illustrating the crystalline nature, which was also confirmed through SAED pattern (inset in Figure 3(c)). The average size distribution of the nanorods was studied through histogram analysis as shown in Figure S2 in Supplementary Information. For obtaining the CoAs nanoparticles the reaction conditions were further altered by injecting a solution of Co_2CO_8 mixed with oleylamine. The addition of a secondary amine altered the phase and solubility of the precursor resulting in nanoparticles as seen in Figure S2(b) in Supplementary Information. These CoAs nanostructures also show interesting magnetic property which evolved as

a function of their morphology and the detailed analysis of these properties has been included in a manuscript submitted by the authors, which also contains other synthesis methods and characterizations of these nanostructures [27].

Figure 4(a) shows the PXRD pattern for MnAs nanoparticles obtained from the reaction of manganese carbonyl with TPA and the comparison with reported MnAs pattern (JCPDS-0072-1065). It should be noted that the product also contained small amount of Mn_3As as impurities visible in the PXRD pattern. Figure 4(a) shows STEM image of the product where nanoparticles were clearly visible with size ranging from 5 to 10 nm, while EDS analysis revealed that the elemental ratio was approximately 1:1 for Mn:As. These MnAs nanoparticles were considerably smaller than the FeAs and CoAs systems. Previously Senevirathne et al. have carried out systematic studies of MnAs nanoparticle synthesis and their magnetic properties [35]. MnAs nanoparticles have magnetostructural properties and are known to have high electromotive force.

CrAs is a ferromagnetic semiconductor [32]. In the Cr-arsenide synthesis process, it was very difficult to isolate the product in the form of a dry powder because of its small size and very well dispersibility in solvents. Upon drying a sticky solid was obtained which could be redispersed in various polar solvents like ethanol, dichloromethane giving a stable dispersion with a green color. Hence in order to characterize these nanoparticles, we performed TEM, EDS, and UV-Vis spectroscopy. PXRD pattern could not be collected due to very small sample quantity and lack of dry powder. Figure 5(a) shows the HRTEM image of ultrasmall CrAs nanoparticles/quantum dots. While TEM and EDS confirmed the particle morphology and composition (~1:1 for Cr:As), Figure 5(b) shows the absorption spectra of the CrAs nanoparticles. There was a strong absorption peak at 560 nm and a band gap of 1.9 eV was estimated from the absorption edge. CrAs shows a band gap of 1.7 eV in the bulk while the minority states at surface show a reduced gap of 1.3 eV [36, 37]. In the current case, the nature and peak positions of the absorption spectra indicate that these are indeed CrAs nanoparticles and that there is a considerable quantum confinement in the nanoparticles resulting in a blue shift of the absorbance band. PL spectra were also collected (λ_{ex} = 380 nm) from a dispersion of the CrAs nanoparticles and shows a broad peak around 500 nm. The origin of emission is most likely the band gap emission which shows similar quantum confinement effect.

Transition metal arsenides are well known for their novel magnetic properties and these nanostructured transition metal arsenides also exhibited interesting magnetic properties. The FeAs and CoAs nanostructures were attracted to the lab magnet to variable extents. The magnetic properties of FeAs and CoAs nanoparticles were specifically measured since they yielded the most pure-phase products. From the temperature-dependent and field-dependent magnetization plots, it could be concluded that the FeAs and CoAs nanoparticles were superparamagnetic with high blocking temperature (T_B) [Figures 6(a) and 6(b)] respectively. Additionally, CoAs nanostructures exhibited signs of ferromagnet-like ordering at low temperature attributed to their anisotropic
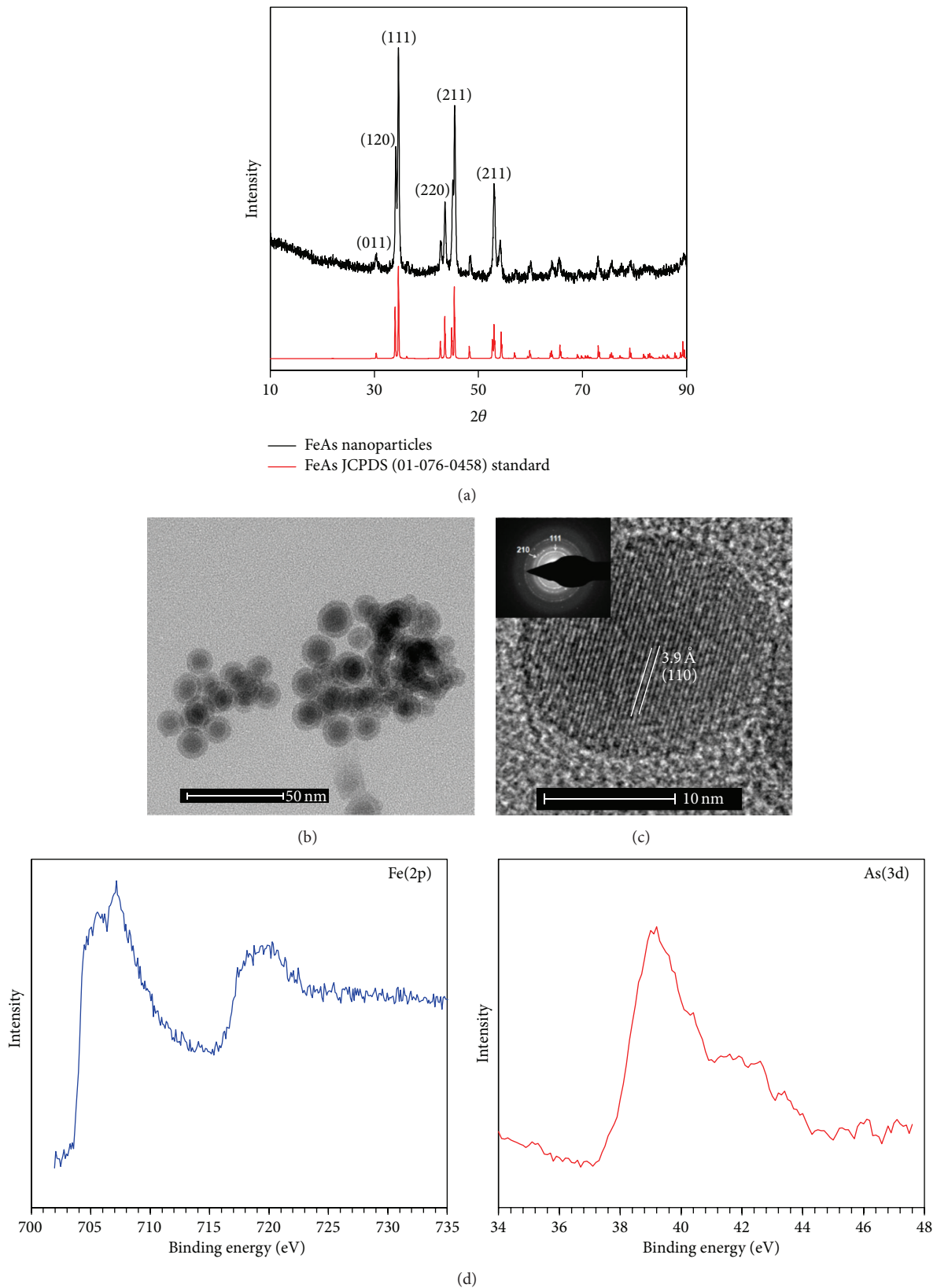
(a)

(b)

(c)

(d)

FIGURE 2: (a) PXRD pattern obtained from the product confirming formation of the FeAs phase. (b) TEM image of the FeAs nanoparticles coated with a carbonaceous shell. (c) HRTEM image of an individual nanoparticle showing single crystalline nature. Inset shows a typical SAED pattern obtained from individual nanoparticle where the diffraction spots could be indexed to the FeAs phase. (d) XPS spectra obtained from the nanoparticles showing Fe2p and As3d peaks.
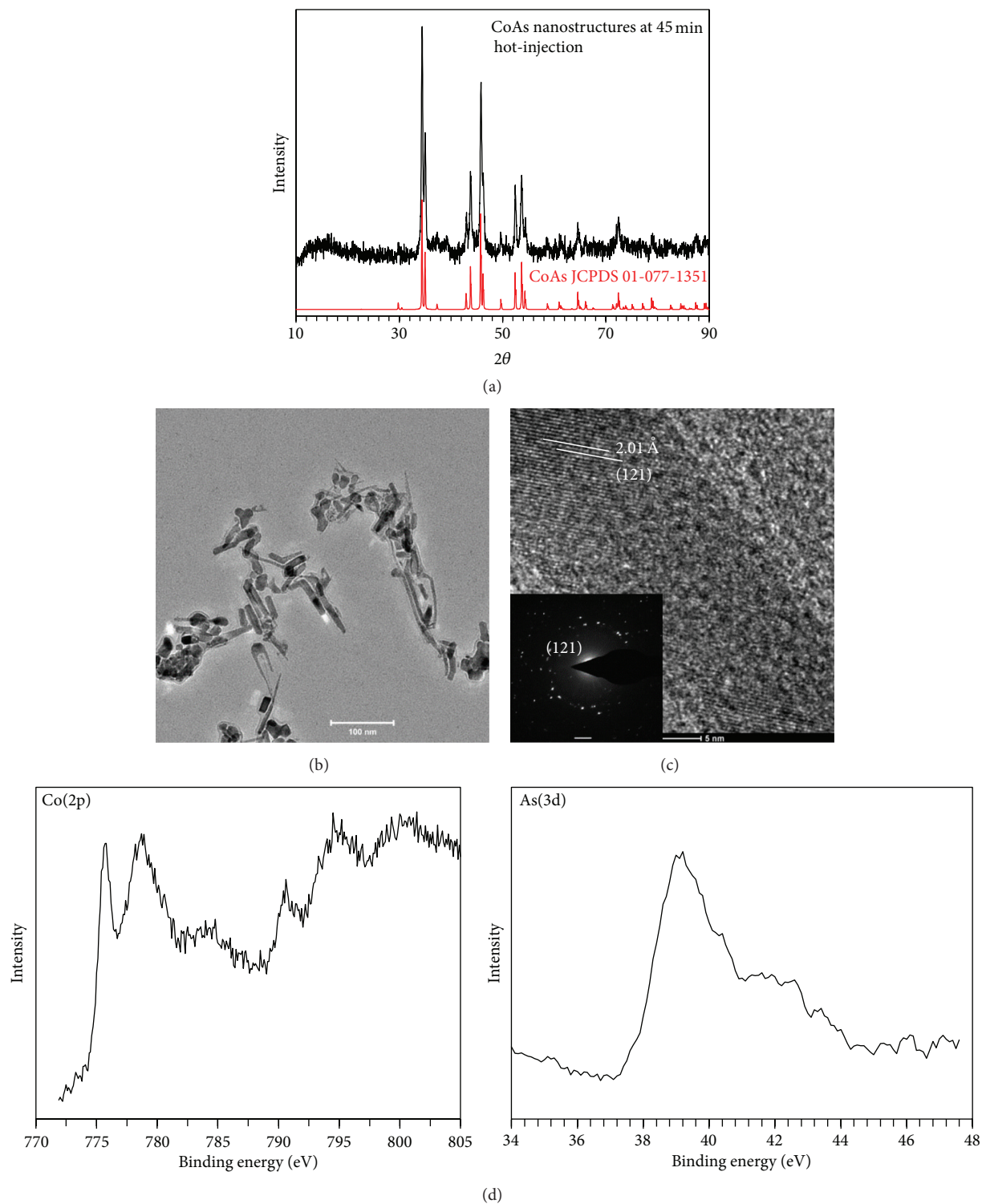
(a)

(b)

(c)

(d)

FIGURE 3: (a) PXRD pattern confirming formation of the CoAs phase. (b) CoAs nanostructures at the initial stages of growth ($t = 10$ min) showing pseudoanisotropic growth; (c) HRTEM of CoAs nanorods showing crystalline nature. Inset shows a typical SAED pattern from the nanorods. (d) XPS spectra obtained from the nanorods showing Co2p and As3d peaks.
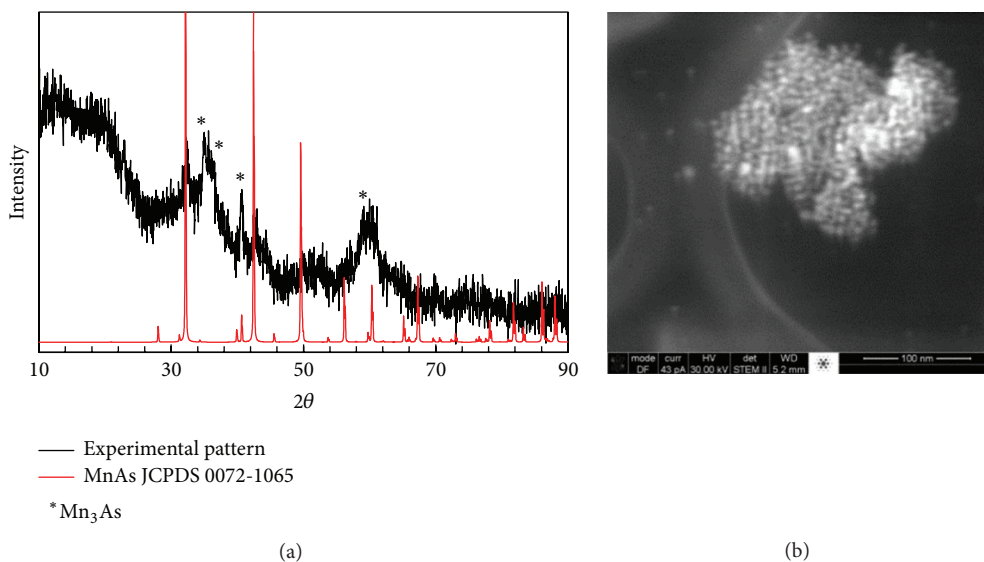
(a)

(b)

FIGURE 4: (a) PXRD pattern of the Mn-arsenide nanostructures. (b) STEM image of the MnAs nanostructures showing particle sizes less than 10 nm.
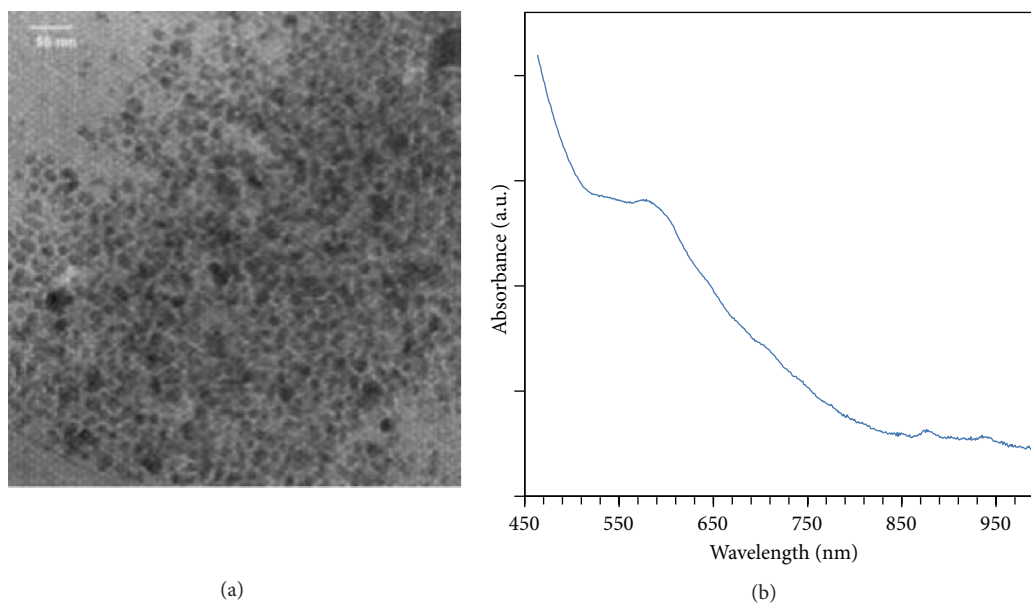

(a)

(b)

FIGURE 5: (a) TEM image of the CrAs nanostructures and (b) shows the UV-Vis spectra. The scale bar in (a) is 50 nm.

shape. It has been predicted that the superparamagnetic T_B can be increased by increasing the shape anisotropy, that is, changing the particle morphology from nanoparticles to 1D nanorods, and the current case with the CoAs nanostructures is a nice illustration of the predictive behavior. A detailed study of these magnetic properties has been discussed by the authors previously [26, 27]. Higher T_B along with larger coercivity increases the applicability of these nanostructures making them suitable for magnetic memory storage and related devices, and the ability to tune T_B through subtle variation in the synthesis methodology as has been shown by this reported procedure will indeed have far-reaching implications.

By conducting several experiments with variable reaction parameters and detailed observations, we have hypothesized a mechanism that can very well explain the evolution of morphology for these nanostructures. The conversion process starts with a burst of nucleation following the addition of $E_x(CO)_y$ at $t = 0$, thereby forming transition metal-rich nuclei capped with HDA. The HDA is typically passivated on the surface of the metal-rich nuclei through affinity between the transition metal and N of HDA, which is classical example of donor-acceptor chemistry. TPA then starts reacting at the surface of the nuclei and the initial layers of EAs forms a coating on the nuclei. The interaction between the growing transition metal-rich nuclei and the amine also affects the
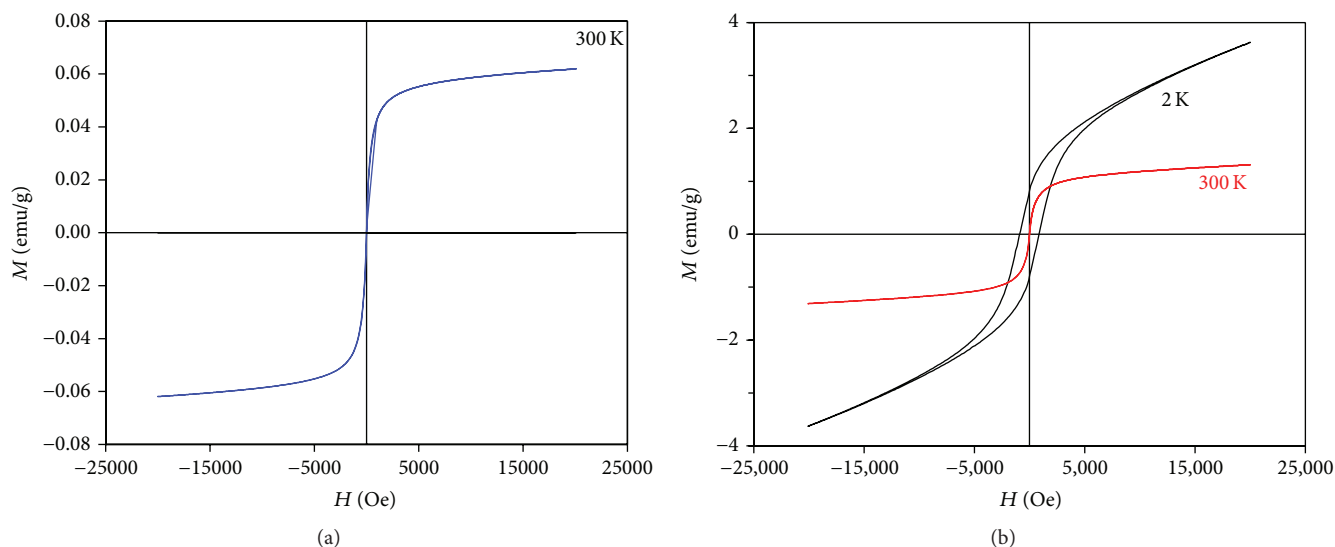
FIGURE 6: Anhysteretic isothermal magnetization showing the superparamagnetic nature of the (a) FeAs and (b) CoAs nanoparticles.

dynamic approach of TPA on the surface. At conditions of constant high temperature (300°C), As diffuses deeper into the nuclei, thereby promoting conversion of the core to EAs. Depending on the critical radius and stability of the nuclei it can then redissolve and reprecipitate. Continuous dissolution and reprecipitation will cause different morphologies to emerge. The negative values of ΔG as calculated from the standard reduction potentials indicate that all these conversions are spontaneous in the reaction medium. However, the negative ΔG does not shed any light on the kinetics of these reactions which determines how fast the nuclei and eventually the nanoparticles are formed. It was observed that the reaction time was shortest for the Co- and Fe-based arsenides which may suggest that their conversion was governed by fast kinetics. CoAs starts showing up in the product within 15 minutes of reaction, while FeAs surfaces at ~40 min. Faster reaction also indicates faster growth-rate of the nuclei which can lead to anisotropic nanostructures in presence of surfactant. In general, we have observed that the propensity towards formation of one-dimensional nanostructures increases as the d electrons availability increases, that is, as we proceed from left to right in the series (Cr to Co). CoAs forms nanorods whereas MnAs and FeAs form nanoparticles with CrAs forming extremely small quantum dots. This can be explained by several factors including the stability/reactivity of the acid-base adduct-like intermediate formed *in situ* through ligand exchange, growth-rate of the nuclei, and rate of conversion. Spontaneous nucleation with slower rate of conversion will expectedly lead to smaller uniformly sized nanoparticles, while continuous nucleation with faster growth will result in larger anisotropic structures. Nucleation will depend on the reactivity of the precursors, in this case the metal carbonyls and the acid-base adduct-like intermediate possibly formed *in situ* as shown in Figure 1. In general Cr-salts are well known for their slower reaction kinetics, which may lead to sluggish reaction, slower growth,

and smaller particles. This can be a classic example where kinetics of the reaction determines the product morphology by controlling the nucleation and growth steps. Faster kinetics of the reaction (arguably in the case of Co, Fe, and Mn to a certain extent) indicates a lower barrier height which will allow the nuclei to redissolve and reprecipitate to form larger particles or anisotropic rod-like structures. Slower kinetics on the other hand indicates a larger barrier height which will inhibit the redissolution step of the nuclei thereby affecting growth as has been observed in the case of CrAs. Even though FeAs reaction shows fast kinetics, the growth of anisotropic structures might be inhibited by the formation of the carbonaceous shell on the FeAs nanoparticles which acts as a protective coating [26]. The formation of this carbonaceous shell depends on the catalytic ability of the transition metal and the FeAs nanostructures exhibited the most predominant carbonaceous shell. A pictorial representation of this growth mechanism is shown in Figure 7 for EAs [E = Cr, Mn, Fe, Co].

4. Conclusions

We have successfully devised a method for the synthesis of nanostructured transition metal arsenides. The novelty of this method is the one-step facile precipitation of the monoarsenides of the 3d transition element series. The chemistry behind this conversion is very facile and involves simple redox chemistry between the metal carbonyls and arsine precursor aided by the amine surfactant which provides a slightly basic medium. We have followed the morphology evolution of the product nanostructures across the transition meal series and observed that reaction kinetics has a more influential role in defining product morphology. Authors are also trying to apply this technique to the main group metals arsenides like InAs and GaAs, which are highly sought after for their application in optoelectronics and photovoltaic devices.
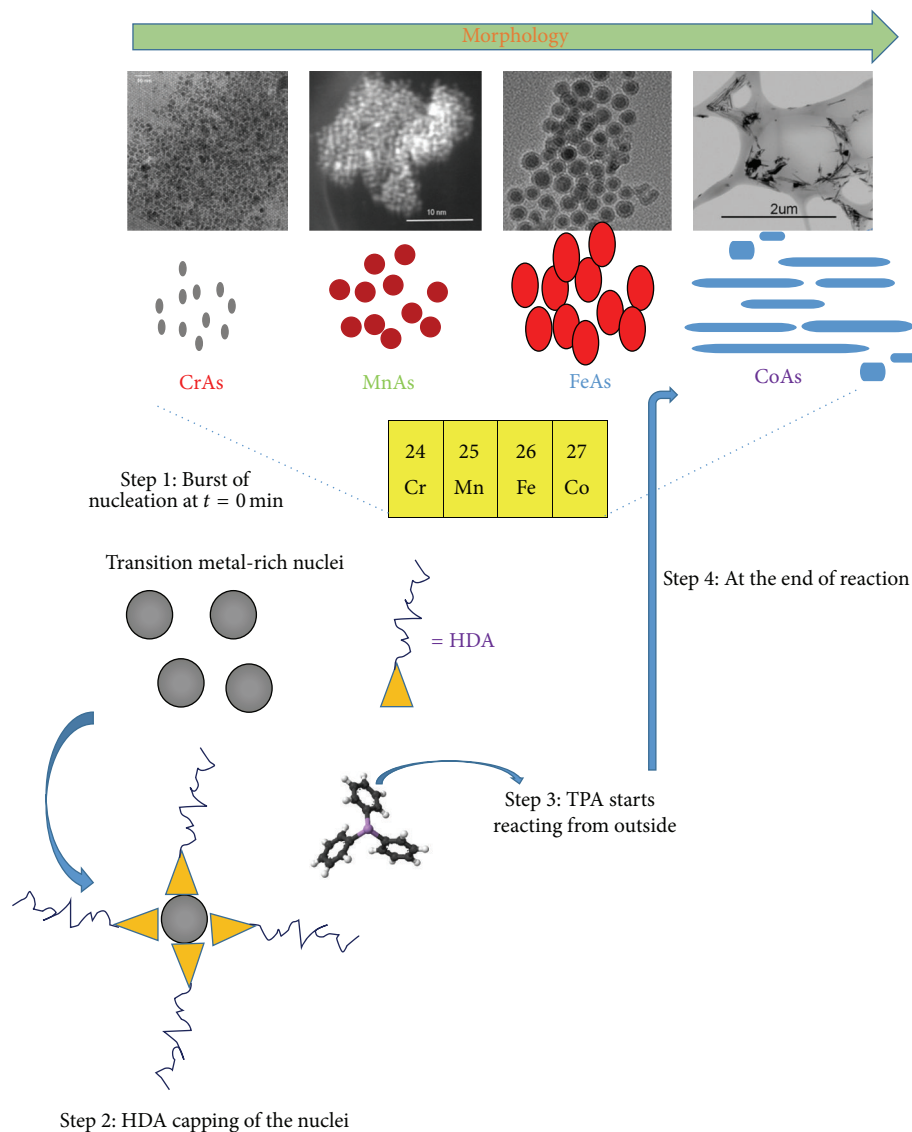
FIGURE 7: Probable growth mechanism and morphology evolution of the *E*As nanostructures.

Conflict of Interests

The authors declare that there is no conflict of interests regarding the publication of this paper.

Acknowledgments

References

[1] J.-Y. Marzin, J.-M. Gérard, A. Izraël, D. Barrier, and G. Bastard, "Photoluminescence of single InAs quantum dots obtained by self-organized growth on GaAs," *Physical Review Letters*, vol. 73, no. 5, pp. 716–719, 1994.

[2] N. P. Dasgupta, J. Sun, C. Liu et al., "25th anniversary article: semiconductor nanowires—synthesis, characterization, and applications," *Advanced Materials*, vol. 26, no. 14, pp. 2137–2183, 2014.

[3] A. T. Howe and P. J. Fensham, "Electronic properties of binary compounds of the first-row transition metals," *Quarterly Reviews, Chemical Society*, vol. 21, no. 4, pp. 507–524, 1967.

[4] J. Suchet, *Crystal Chemistry and Semiconduction in Transition Metal Binary Compounds*, Elsevier, 2012.

[5] M.-P. Bichat, F. Gillot, L. Monconduit et al., "Redox-induced structural change in anode materials based on tetrahedral $(MPn_4)^{x-}$ transition metal pnictides," *Chemistry of Materials*, vol. 16, no. 6, pp. 1002–1013, 2004.

[6] W.-H. Xie, B.-G. Liu, and D. G. Pettifor, "Half-metallic ferromagnetism in transition metal pnictides and chalcogenides with wurtzite structure," *Physical Review B*, vol. 68, no. 13, Article ID 134407, 2003.

[7] L. Chioncel, M. I. Katsnelson, G. A. De Wijs, R. A. De Groot, and A. I. Lichtenstein, "Tunable spin transport in CrAs: role of correlation effects," *Physical Review B*, vol. 71, no. 8, Article ID 085111, 2005.

[8] B. Sanyal, L. Bergqvist, and O. Eriksson, "Ferromagnetic materials in the zinc-blende structure," *Physical Review B—Condensed Matter and Materials Physics*, vol. 68, no. 5, Article ID 054417, 2003.

[9] L. Häggström, A. Gustavsson-Seidel, and H. A. Fjellvåg, "A mössbauer study of helimagnetic FeAs," *Europhysics Letters*, vol. 9, no. 1, pp. 87–92, 1989.

[10] F. Matsukura, H. Ohno, and T. Dietl, "III-V ferromagnetic semiconductors," in *Handbook of Magnetic Materials*, vol. 14, chapter 1, pp. 1–87, Elsevier Science, 2002.

[11] C. Uher, "Chapter 5 Skutterudites: prospective novel thermoelectrics," *Semiconductors and Semimetals*, vol. 69, pp. 139–253, 2001.

[12] A. Vetcher, A. Kattwinkel, C. Kleeberg, E. Kraus, P. Fröbel, and K. Bärner, "The thermoelectric power of some magnetically ordered transition metal pnictides," *Physica Status Solidi (A) Applied Research*, vol. 166, no. 2, pp. 843–851, 1998.

[13] K. Zhou, S. Jiang, B. Wang et al., "Combined effect of transition metal phosphide (M_xP_y, M=Ni, Co, and Cu) and intumescent flame retardant system on polypropylene," *Polymers for Advanced Technologies*, vol. 25, no. 7, pp. 701–710, 2014.

[14] I. I. Abu and K. J. Smith, "HDN and HDS of model compounds and light gas oil derived from Athabasca bitumen using supported metal phosphide catalysts," *Applied Catalysis A: General*, vol. 328, no. 1, pp. 58–67, 2007.

[15] S. T. Oyama, "Novel catalysts for advanced hydroprocessing: transition metal phosphides," *Journal of Catalysis*, vol. 216, no. 1-2, pp. 343–352, 2003.

[16] C. Stinner, R. Prins, and T. Weber, "Binary and ternary transition-metal phosphides as HDN catalysts," *Journal of Catalysis*, vol. 202, no. 1, pp. 187–194, 2001.

[17] V. Zuzaniuk and R. Prins, "Synthesis and characterization of silica-supported transition-metal phosphides as HDN catalysts," *Journal of Catalysis*, vol. 219, no. 1, pp. 85–96, 2003.

[18] R.-K. Chiang and R.-T. Chiang, "Formation of hollow Ni_2P nanoparticles based on the nanoscale Kirkendall effect," *Inorganic Chemistry*, vol. 46, no. 2, pp. 369–371, 2007.

[19] D. Johrendt and R. Pöttgen, "Pnictide oxides: a new class of high-T_C superconductors," *Angewandte Chemie—International Edition*, vol. 47, no. 26, pp. 4782–4784, 2008.

[20] Y. Li, M. A. Malik, and P. O'Brien, "Synthesis of single-crystalline CoP nanowires by a one-pot metal-organic route," *Journal of the American Chemical Society*, vol. 127, no. 46, pp. 16020–16021, 2005.

[21] S. C. Perera, G. Tsoi, L. E. Wenger, and S. L. Brock, "Synthesis of MnP nanocrystals by treatment of metal carbonyl complexes with phosphines: a new, versatile route to nanoscale transition metal phosphides," *Journal of the American Chemical Society*, vol. 125, no. 46, pp. 13960–13961, 2003.

[22] A. Addamiano, "On the preparation of the phosphides of aluminum, gallium and indium," *Journal of the American Chemical Society*, vol. 82, no. 7, pp. 1537–1540, 1960.

[23] J. Lu, Y. Xie, X. Jiang, W. He, and G. Du, "A safe sonochemical route to iron, cobalt and nickel monoarsenides," *Journal of Materials Chemistry*, vol. 11, no. 12, pp. 3281–3284, 2001.

[24] X. M. Zhang, C. Wang, X. F. Qian, Y. Xie, and Y. T. Qian, "Synthesis of nanocrystalline iron monoarsenide via a reductive recombination pathway," *Journal of Solid State Chemistry*, vol. 144, no. 2, pp. 237–239, 1999.

[25] K. L. Stamm, J. C. Garno, G.-Y. Liu, and S. L. Brock, "A general methodology for the synthesis of transition metal pnictide nanoparticles from pnictate precursors and its application to iron-phosphorus phases," *Journal of the American Chemical Society*, vol. 125, no. 14, pp. 4038–4039, 2003.

[26] P. Desai, K. Song, J. Koza, A. Pariti, and M. Nath, "Soft-chemical synthetic route to superparamagnetic FeAs@C core-shell nanoparticles exhibiting high blocking temperature," *Chemistry of Materials*, vol. 25, no. 9, pp. 1510–1518, 2013.

[27] P. Desai, N. Ashokaan, J. Masud, A. Pariti, and M. Nath, "Synthesis and magnetic properties of superparamagnetic CoAs nanostructures," *Materials Research Express*, vol. 2, no. 3, Article ID 036102, 2015.

[28] R. H. Crabtree, *The Organometallic Chemistry of the Transition Metals*, Wiley, 2001.

[29] P. Macchi, L. Garlaschelli, S. Martinengo, and A. Sironi, "Characterization of the solid-solid phase transition of $Co_2(CO)_6(AsPh3)_2$," *Inorganic Chemistry*, vol. 37, no. 24, pp. 6263–6268, 1998.

[30] H. Schumann, J. M. M. Smits, and P. T. Beurskens, "Crystal and molecular structure of [dicarbonyl (η-cyclopentadienyl)ferrio]triphenylarsine tetrafluoroborate, $[(C_6H_5)_3AsFe(CO)_2(C_5H_6)][BF_4]$," *Journal of Crystallographic and Spectroscopic Research*, vol. 19, no. 6, pp. 1033–1039, 1989.

[31] B. Saparov, J. E. Mitchell, and A. S. Sefat, "Properties of binary transition-metal arsenides (TAs)," *Superconductor Science and Technology*, vol. 25, no. 8, Article ID 084016, 2012.

[32] K. Selte, A. Kjekshus, W. E. Jamison, A. F. Andresen, J. E. Engebretsen, and L. Ehrenberg, "Magnetic structure and properties of CrAs," *Acta Chemica Scandinavica*, vol. 25, pp. 1703–1714, 1971.

[33] K. Selte, A. Kjekshus, J. Sletten et al., "Crystal structure of FeAs," *Acta Chemica Scandinavica*, vol. 23, pp. 2047–2054, 1969.

[34] K. Motizuki, "Recent advances in the theory of magnetism of NiAs-type transition-metal chalcogenides and pnictides," *Journal of Magnetism and Magnetic Materials*, vol. 70, no. 1–3, pp. 1–7, 1987.

[35] K. Senevirathne, R. Tackett, P. R. Kharel, G. Lawes, K. Somaskandan, and S. L. Brock, "Discrete, dispersible mnas nanocrystals from solution methods: phase control on the nanoscale and magnetic consequences," *ACS Nano*, vol. 3, no. 5, pp. 1129–1138, 2009.

[36] J. I. Lee and S. C. Hong, "Electronic structures, magnetism, and half-metallicities of CrAs(110)," *IEEE Transactions on Magnetics*, vol. 42, no. 10, pp. 2936–2938, 2006.

[37] A. Bala, P. Singh, T. Nautiyal, and S. Auluck, "Magnetic CrX and MnX (X = Si, Ge, and As) nanowires: stability enhancement and linearization," *Journal of Alloys and Compounds*, vol. 547, pp. 138–146, 2013.